Two sources of asymmetry-induced transport

D. L. Eggleston
Physics Department, Occidental College, Los Angeles, California 90041, USA

(Received 17 January 2012; accepted 30 March 2012; published online 30 April 2012)

A single-particle computer code with collisional effects is used to study asymmetry-induced radial transport of a non-neutral plasma in a coaxial Malmberg-Penning trap. Following the time variation of the mean change and mean square change in radial position allows for the calculation of the radial drift velocity v_D and the diffusion coefficient D as defined by the radial flux equation $\Gamma = -D\frac{dn_0}{dr} + n_0 v_D$. For asymmetries of the form $\phi_1(r)\cos(kz + \omega t - l\theta)$ and periodic boundary conditions, the transport coefficients obtained match those predicted by resonant particle transport theory where the transport is produced by particles with velocities near $\pm(l\omega_R - \omega)/k$, with ω_R being the azimuthal rotation frequency. For asymmetries of the form $\phi_1(r)\cos(kz)\cos(\omega t - l\theta)$ and low collision frequency, there is a second contribution to the transport produced by low velocity particles axially trapped in the asymmetry potential. These produce a stronger variation of D with ω with a peak at $\omega = \omega_R$. The width of the peak $\Delta\omega$ increases with center conductor bias and decreases with radius, while the height shows the opposite behavior. The transport due to axially trapped particles is typically comparable to or larger than that from resonant particles. This second contribution to the transport may explain the discrepancies between experiments and resonant particle theory. © *2012 American Institute of Physics*. [http://dx.doi.org/10.1063/1.4707395]

I. INTRODUCTION

The Malmberg-Penning non-neutral plasma trap has been used for some time for basic studies of plasma transport. Once the base pressure is low enough to minimize electron-neutral transport, the confinement is limited by electric and magnetic fields that break the cylindrical symmetry of the trap and produce radial drifts. This asymmetry-induced transport has been studied experimentally by a number of people,[1–9] but detailed comparisons of the predictions of resonant particle transport theory[10] with experiment[7] show serious discrepancies. It seems clear that some important physics is missing from the theory.

In a previous paper,[11] we examined the dynamics of particles in a coaxial Malmberg-Penning trap with prescribed asymmetric electric fields using a simple single-particle computer simulation. We found that, for a single helical asymmetry with periodic boundary conditions, significant motion in the radial direction was restricted to those particles near the resonant velocity, and that both the location and the width of this resonance were consistent with analytical theory. When a standing wave asymmetry was used, however, additional dynamical behaviors were observed not included in the theory. The most striking of these was the existence of a low-velocity population of particles with large radial excursions and restricted axial motion in the lab frame. In addition, a larger region of stochastic motion occurred where the resonant regions of the two constituent counter-propagating helical waves overlapped.

Although these results were suggestive, the transport coefficients resulting from the new dynamical motions could not be determined. To find these coefficients, we have now added collisions to our code. By following the time variation of the mean change and mean square change in radial position, we can obtain, respectively, the drift velocity v_D and the diffusion coefficient D as defined by the radial flux equation $\Gamma = -D\frac{dn_0}{dr} + n_0 v_D$, where n_0 is the particle density. As expected from the dynamical studies, v_D and D generally match resonant particle transport theory for the simplest helical asymmetry with periodic boundary conditions. For the more realistic standing wave asymmetries, however, there are two contributions to the transport at low collision frequencies. The first is that given by resonant particle transport theory and is produced by particles with velocity near $\pm(l\omega_R - \omega)/k$, where ω_R is the azimuthal rotation frequency, ω is the asymmetry frequency, and k is the axial wavenumber. The second contribution is produced by the low velocity particles that are axially trapped in the asymmetry potential. These produce a stronger variation of D with ω with a peak near $\omega = \omega_R$. The width of the peak $\Delta\omega$ increases with center wire bias and decreases with radius, while the height shows the opposite behavior. The transport due to these axially trapped particles is typically comparable to or larger than that from resonant particles. We also find that the relationship between v_D and D given by the Einstein relation fails for this contribution to the transport.

II. SIMULATION DETAILS

Our code is constructed to model our experimental device, which is shown in Fig. 1. Low density electrons are confined in the central region of length L between the negatively biased injection gate and dump gate. In order to maintain an azimuthal $E \times B$ drift comparable to a higher density plasma, a negatively biased wire is stretched along the axis of the device. The uniform axial magnetic field B providing radial confinement is strong enough that the gyroradius is much smaller than the wall radius R. The walls of the confinement region are divided into forty sectors (five axial divisions S1-S5 with eight azimuthal divisions each), which

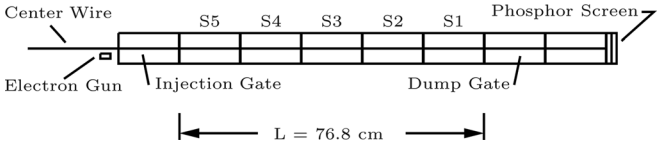

FIG. 1. Schematic of the Occidental College Trap. The usual plasma column is replaced by a biased wire to produce the basic dynamical motions in low density electrons injected from an off-axis gun.

allows application of an asymmetric electric field. The voltages applied to these sectors are typically chosen so that the field consists primarily of a single Fourier mode. The remaining details of the experiment are given elsewhere.[7]

The code follows the dynamics of single particles in prescribed fields; inter-particle fields are not included. The prescribed fields are set by the center wire potential and the asymmetric potential. The center wire potential is given by

$$\phi_0(r) = \phi_{cw}\frac{\ln(R/r)}{\ln(R/a)}, \tag{1}$$

where ϕ_{cw} is the bias of the center wire, R is the radius of the wall, and a is the radius of the center wire. The asymmetric potential is chosen to be either a helical wave

$$\phi_{hel}(r,\theta,z,t) = \phi_1(r)\cos(kz - l\theta + \omega t) \tag{2}$$

or an axially standing wave

$$\phi_{sw}(r,\theta,z,t) = 2\phi_1(r)\cos(kz)\cos(-l\theta + \omega t). \tag{3}$$

In Eqs. (2) and (3), $k = n\pi/L$ and n is the axial wavenumber, l is the azimuthal wavenumber, ω is the asymmetry frequency, and z is measured from one end of the confinement region. The amplitude $\phi_1(r)$ is taken to be of the form $\phi_{10}(r/R)^l$ where ϕ_{10} is a constant. This form closely approximates the exact vacuum solution.

The particle motions in the code are governed by

$$\frac{dr}{dt} = v_r \quad r\frac{d\theta}{dt} = v_\theta \quad \frac{dz}{dt} = v_z \quad \frac{dv_z}{dt} = \frac{qE_z}{m} - \nu v_z, \tag{4}$$

where ν is the electron-electron collision frequency. For typical experimental conditions, the gyroradius is much smaller than the wall radius R and the cyclotron frequency is much larger than all other dynamical frequencies. We thus ignore the cyclotron motion and follow the motion of the guiding center. In this drift approximation, v_r and v_θ are given by

$$v_r = \frac{E_\theta}{B} \quad v_\theta = -\frac{E_r}{B}. \tag{5}$$

The electric fields are obtained from the prescribed potentials: $E_r = -\frac{\partial\phi}{\partial r}, E_\theta = -\frac{1}{r}\frac{\partial\phi}{\partial\theta}$, and $E_z = -\frac{\partial\phi}{\partial z}$. For comparisons with analytic theory, we note that the zeroth order variation of E_r defines the rotation frequency ω_R

$$\omega_R = -\frac{E_{r0}}{rB} = \frac{-\phi_{cw}}{r^2 B\ln(R/a)} \tag{6}$$

where in the last step, we have used Eq. (1). Since ϕ_{cw} is typically negative, ω_R is positive.

Collisions are included according to the Langevin prescription.[13,14] This prescription has two parts. First, a drag term $-\nu v_z$ is included in the equation of motion for v_z in Eq. (4). Second, after each time step Δt, a velocity Δv is added to v_z. The value of Δv is generated with a random number routine that gives values uniformly distributed over the range $-v_0 \le \Delta v \le v_0$, where v_0 is related to the electron temperature T and the collision frequency ν by (see Appendix A)

$$v_0^2 = \frac{6kT}{m}\nu\Delta t. \tag{7}$$

Initially, all particles are placed at the same radius, but are distributed in z, θ, and v_z. We typically use 64 512 particles (32 z-values × 16 θ-values × 126 v_z-values). To account for the variation in particle density in a Maxwellian velocity distribution, the particles are assigned a weighting factor $W_i = \exp[-(v_{zi}/v_{th})^2]$, where v_{th} is the thermal velocity and i is the particle number index.

Equations (4) and (5) are solved using a fourth-order Runge-Kutta method.[12] To maintain precision, the velocities are scaled to 10^6 cm/s, the asymmetry frequency ω is scaled to 10^6 rad/s, and time t is scaled to 10^{-6} s. Parameters are chosen to match our typical experimental conditions and unless otherwise specified are $B = 364\,\mathrm{G}, L = 76.8\,\mathrm{cm}$, $R = 3.87\,\mathrm{cm}$, $a = 0.007\,\mathrm{in}$, $\phi_{cw} = -80\,\mathrm{V}$, $\phi_{10} = 0.1\,\mathrm{V}$, and $n = l = 1$.

The code has two options for the ends of the trap: periodic boundaries or specular reflection. For periodic boundaries, the axial position of the particle can range from $z = -L$ to $z = L$. Particles reaching $z = L$ are shifted to $z = -L$ and vice versa. For specular reflection, the axial position ranges from $z = 0$ to $z = L$. At the ends, the particle simply reverses axial direction as if bouncing off of an infinite potential.

The transport coefficients are determined by following two quantities:

$$\langle\Delta r\rangle \equiv \frac{1}{W}\sum_{i=1}^{M} W_i[r_i(t) - r_i(0)] \tag{8}$$

and

$$\langle(\Delta r)^2\rangle \equiv \frac{1}{W}\sum_{i=1}^{M} W_i[r_i(t) - r_i(0)]^2. \tag{9}$$

Here, M is the total number of particles and $W = \sum W_i$ is the sum over weighting factors. Assuming a radial particle flux Γ of the form

$$\Gamma = -D\frac{dn_0}{dr} + n_0 v_D, \tag{10}$$

the drift velocity v_D is given by

$$v_D = \frac{d}{dt}\langle\Delta r\rangle \tag{11}$$

and the diffusion coefficient D by

$$D = \frac{1}{2}\frac{d}{dt}\left[\langle(\Delta r)^2\rangle - \langle\Delta r\rangle^2\right]. \quad (12)$$

We find that the quantities $\langle\Delta r\rangle$ and $\langle(\Delta r)^2\rangle$ defined by Eqs. (8) and (9) vary with time. Typical behavior is shown in Fig. 2. Since our desired transport coefficients v_D and D depend on these quantities, we must decide how long to run the simulation and when to evaluate Eqs. (11) and (12). The initial oscillations shown in Fig. 2 can be attributed to the radial motions of trapped particles, since their frequency matches the trapped particle oscillation frequency ω_T defined in Sec. III. These oscillations damp out in time either due to phase mixing or collisional scattering. On the other hand, for long run times, some particles will move significantly away from their initial position and their subsequent motion may not be consistent with a local approximation. For the parameters of these studies, the phase mixing is complete by $\omega_T T \approx 10$, where T is the run time. The collisional scattering of trapped particles requires $\nu_{\text{eff}} T \approx 1$ while the scattering of bulk particles requires $\nu T \approx 1$. For the smaller values of ν, this last requirement gives the largest value of T, so we use it to set the run time. For the largest values of ν, $\omega_T T \approx 10$ is used to set T.

III. SUMMARY OF RESONANT PARTICLE TRANSPORT THEORY

In Sec. IV, we will compare the simulation to resonant particle transport theory, which is summarized here. A more complete presentation of the theory is given in Ref. 10. The theory assumes a cylindrical geometry with an axial magnetic field B. Under the strong magnetic field conditions typical of most non-neutral plasmas, the basic equations are Poisson's equation and the drift kinetic equation with a collision operator, and the boundary conditions on the conducting walls. A plasma of length L with flat ends is assumed and end effects are ignored. This allows for the linearization of the potential as $\phi(r,\theta,z,t) = \phi_0(r) + \phi_1(r,\theta,z,t)$, where

$$\phi_1(r,\theta,z,t) = \sum_{n,l,\omega} \phi_{nl\omega}(r)\cdot\exp\left[i\left(\frac{n\pi}{L}z + l\theta - \omega t\right)\right] \quad (13)$$

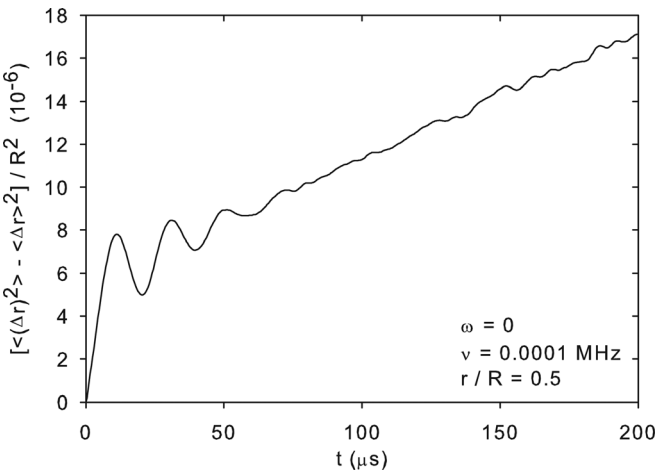

FIG. 2. Initial time variation of the scaled mean square change in radial position showing trapped particle oscillations.

is the asymmetry potential decomposed into Fourier modes of amplitude $\phi_{nl\omega}(r)$ and characterized by axial mode n, azimuthal mode l, and angular frequency ω. The triple sum includes both negative and positive values of n, l, and ω. The Fourier amplitudes can be computed from a given asymmetry potential from the equation

$$\phi_{nl\omega}(r) = \int_{-L}^{L}\frac{dz}{2L}\int_0^{2\pi}\frac{d\theta}{2\pi}\int_0^{\tau}\frac{dt}{\tau}\exp\left[i\left(\frac{n\pi}{L}z + l\theta - \omega t\right)\right] \times \phi_1(r,\theta,z,t). \quad (14)$$

The resulting radial particle flux can be written in the form

$$\Gamma = -\sum_{n,l,\omega}\left[D_{nl\omega}\frac{dn_0}{dr} + n_0 V_{nl\omega}\right]. \quad (15)$$

For simplicity, we have assumed here that the temperature T is constant with radius, as it is in the simulation. Some details in the evaluation of Eq. (15) are given in Appendix B.

The form of the diffusion coefficients $D_{nl\omega}$ and drift velocities $V_{nl\omega}$ depends on the relative size of an effective collision frequency ν_{eff} and the oscillation frequency ω_T of particles trapped in the moving frame of the asymmetry potential. Here, $\nu_{\text{eff}}^3 \approx \nu\left(\frac{n\pi\bar{v}}{L}\right)^2$ and

$$\omega_T^2 = \left[\frac{e}{m}\left(\frac{n\pi}{L}\right)^2 - \frac{cl^2}{rB}\frac{d\omega_R}{dr}\right]\phi_{nl\omega}(r), \quad (16)$$

where ω_R is the azimuthal $E\times B$ rotation frequency of the plasma column. When $\nu_{\text{eff}} \gg \omega_T$, frequent collisions interrupt the trapped particle orbits and the basic radial step is the radial $E\times B$ velocity multiplied by the time between collisions. Deviations from unperturbed orbits are small, and a perturbation approach is appropriate. This is called the plateau regime. When $\nu_{\text{eff}} < \omega_T$, a trapped particle can complete at least one oscillation before a collision knocks it out of resonance. Now, the basic radial step is the radial extent of the drift during a trapping oscillation, and the orbits are fully nonlinear. A heuristic derivation of the resulting radial flux is often employed for this "banana" regime. For the plateau regime,

$$D_{nl\omega} = \frac{1}{\sqrt{2\pi\bar{v}^2}}\frac{L}{|n|}\left|\frac{cl\phi_{nl\omega}(r)}{rB}\right|^2 e^{-x^2} \quad (17)$$

while for the banana regime

$$D_{nl\omega} = \frac{1}{\sqrt{2\pi}}\frac{\nu\left(\frac{L}{n\pi}\right)^2\left(\frac{l\bar{v}}{r\omega_c}\right)^2\left(\frac{e\phi_{nl\omega}(r)}{T}\right)^{1/2}}{\left[1-\left(\frac{lL}{n\pi}\right)^2\frac{1}{r\omega_c}\frac{d\omega_R}{dr}\right]^{3/2}}e^{-x^2}. \quad (18)$$

The variable x is equal to $v_{res}/\sqrt{2}\bar{v}$, where

$$v_{res} = \frac{L}{n\pi}(\omega - l\omega_R) \quad (19)$$

is the resonant velocity for the asymmetry mode n, l, ω. The symbols $n_0, \bar{v}, \omega_c$, and ν denote the electron density, thermal

velocity, cyclotron frequency, and the electron-electron collision frequency, respectively. In both regimes, the drift velocity $V_{nl\omega}$ is given by

$$V_{nl\omega} = \frac{r\omega_c}{l\bar{v}^2}(\omega - l\omega_R)D_{nl\omega}. \quad (20)$$

For the static case ($\omega = 0$), Eq. (20) reduces to the Einstein relation.

IV. RESULTS

A. Helical asymmetry with periodic boundary conditions

We begin by examining the case of a helical asymmetry as given by Eq. (2), subject to periodic boundary conditions. In our previous work, we found that the particle dynamics for this case were consistent with expectations from resonant particle transport theory, namely, that the particles having the largest radial excursions had velocities in the range $v_{res} \pm 2L\omega_T/n\pi$. We thus expect the transport coefficients will agree with resonant particle transport theory. We test this expectation by examining the absolute magnitude of the diffusion coefficient D, its dependence on collision frequency ν and asymmetry frequency ω, and by comparing the magnitude and ω-dependence of the drift velocity v_D found via Eq. (11) with that predicted by Eq. (20).

In Fig. 3, the filled circles show the value of D obtained from the simulation as a function of collision frequency. For this example, we used $r/R = 0.5$ and $\omega = 0$. The dashed lines show the predictions of resonant particle transport theory for the plateau and banana regimes (Eqs. (17) and (18), respectively). The comparison is absolute and there are no adjustable parameters. There is good agreement between simulation and theory in terms of the absolute value of D, its dependence on ν, and the predicted division between plateau and banana regimes.

Figure 4(a) shows the dependence of D on asymmetry frequency ω for $r/R = 0.5$ and two values of the collision frequency, one in the plateau regime and one in the banana regime. The open and closed circles show the simulation results. The solid lines show the predicted $\exp(-x^2)$ dependence (see Eqs. (17) and (18)) with the peak value fit to the simulation results. Agreement is good.

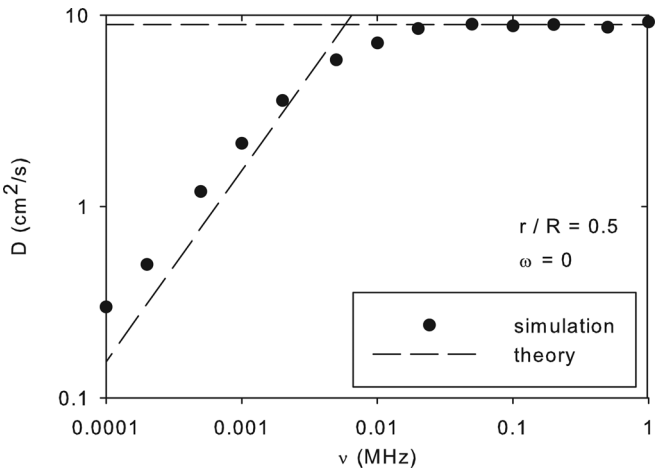

FIG. 3. Diffusion coefficient D vs. collision frequency ν for a helical asymmetry. The filled circles show the value obtained from the simulation. The dashed lines show the predictions of resonant particle transport theory for the plateau and banana regimes.

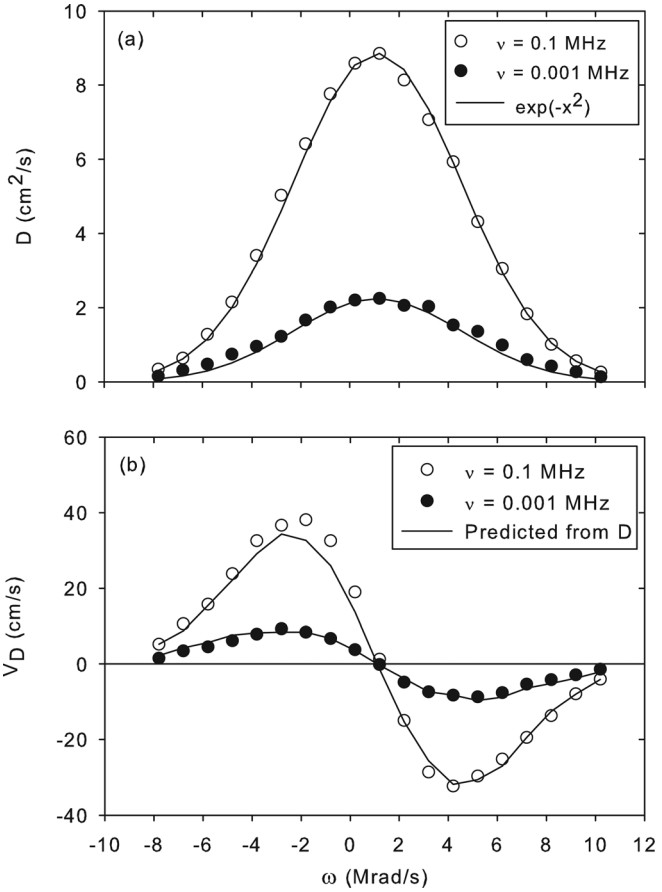

FIG. 4. The dependence of the transport coefficients on asymmetry frequency ω for a helical asymmetry. The open and closed circles show the simulation results for two values of the collision frequency ν. (a) The diffusion coefficient D. The solid lines show the predicted $\exp(-x^2)$ dependence. (b) Drift velocity v_D vs. asymmetry frequency ω. The solid lines show the prediction of the Einstein relation Eq. (20).

The symbols in Fig. 4(b) show the values of v_D obtained from the simulation for the same two values of ν, again as a function of ω. Here, the solid lines show the prediction for v_D obtained by using Eq. (20) and the values of D from Fig. 4(a). Again, we see good agreement between simulation and theory.

B. Standing wave asymmetry

We now turn to consider the transport produced by a standing wave asymmetry of the form given by Eq. (3), with specular reflection at the ends. This asymmetry is the simplest case of the type more representative of experiments where the z-variation does not appear in combination with the θ and t variations. It is for this case that we previously observed particle dynamics not included in resonant particle theory. Here, we find that this does indeed affect D and v_D.

It is easy to show that a standing wave asymmetry of the form in Eq. (3) can be written as two helical asymmetries of the form in Eq. (2) with oppositely signed n values. Changing the sign of n, however, does not change either the

diffusion coefficient or drift velocity in resonant particle theory. Thus, theory predicts that our standing wave asymmetry will simply produce twice the transport of a single helical asymmetry. Consistent with this, the frequency dependence of the transport coefficients resembles Fig. 4, with the important exception shown in Fig. 5. Here, we plot the simulation results for the transport coefficients versus the asymmetry frequency for parameter choices $r/R = 0.5$ and $\nu = 0.001$ MHz. Note the change of horizontal scale on this plot compared with Fig. 4. The solid symbols are the results for the standing wave asymmetry while the open symbols give the values obtained by doubling the result for a single helical asymmetry, thus giving the prediction of resonant particle theory. Clearly, for this range of frequencies, D is significantly larger than expected from resonant particle theory and has a stronger variation with frequency.

The results for v_D also disagree with theory, as shown in Fig. 5(b). Here, the discrepancy between simulation and theory is even more pronounced, with v_D from the simulation 10-50 times larger than predicted. In addition, the solid line shows the prediction for v_D obtained by using Eq. (20) and the standing wave values of D from Fig. 5(a). This also disagrees with the simulation, showing the breakdown of our Einstein relation for this case.

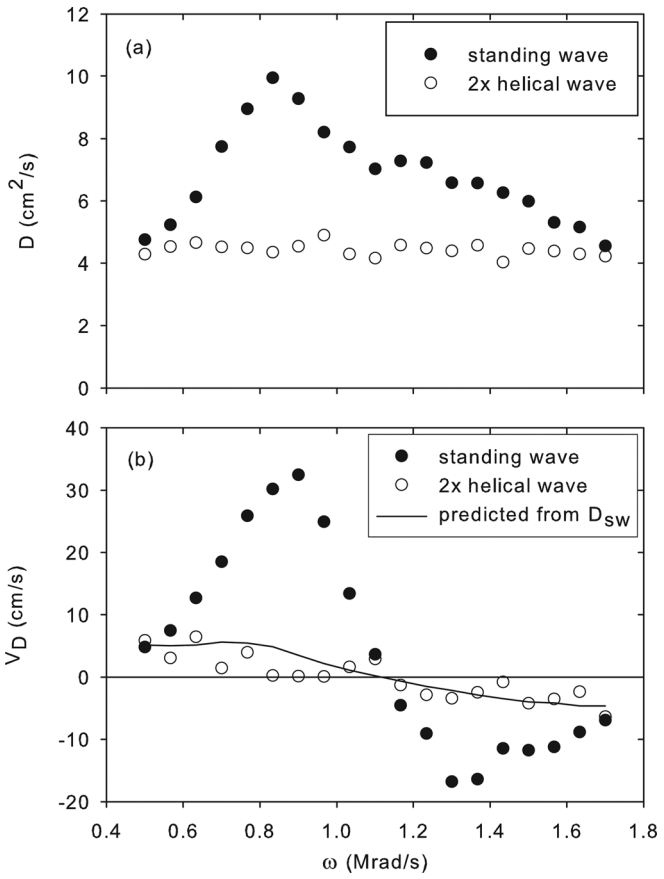

FIG. 5. The dependence of transport coefficients on asymmetry frequency ω for a standing wave asymmetry (solid circles). For comparison, twice the diffusion coefficient for a helical asymmetry is shown by the open circles. Here, $r/R = 0.5$ and $\nu = 0.001$ MHz. Note the change in the range of ω compared with Fig. 4. (a) Diffusion coefficient D. (b) Drift velocity v_D vs. asymmetry frequency ω. The solid line shows the prediction of the Einstein relation Eq. (20).

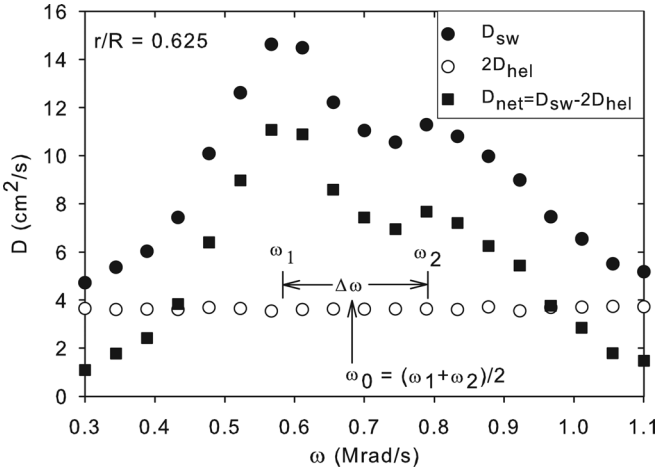

FIG. 6. Parameters used to characterize the transport for the standing wave asymmetry are shown.

It is interesting to note that the observed enhancement in D and v_D occurs only for small collision frequencies. When we repeat the simulation runs with $\nu = 0.1$ MHz, the enhancement vanishes and the transport coefficients for the standing wave asymmetry match those for a helical asymmetry doubled.

The data displayed in Figs. 5(a) and 5(b) show that, for the standing wave asymmetry and low collision frequency, there is "extra" transport above what is expected from resonant particle theory and that this extra transport occurs only for a range of frequencies. Exploring the parameter space of our simulation, we find that the characteristics of the extra transport vary with radius and center wire bias. To quantify this variation, we have defined parameters as shown in Fig. 6. The observed variation of D with frequency has two local peaks, and we define the frequencies at these peaks as ω_1 and ω_2. The average of these, defining the center of the overall variation, we call ω_0, and the difference in frequencies, defining the width of the overall variation, we call $\Delta\omega$. Finally, we characterize the amount of extra transport by D_{net}, the difference between D obtained for the standing wave asymmetry and twice the D obtained for a single helical asymmetry.

Figure 7 shows how the center frequency ω_0 varies with scaled radius r/R and center wire bias ϕ_{cw}. The filled symbols are the simulation data and the lines are plots of ω_R obtained from Eq. (6). The plot supports the conclusion that $\omega_0 = \omega_R$. This was expected from our work on particle dynamics,[11] since it was for asymmetry frequencies near ω_R that large radial excursions in axially trapped particles was observed. We conclude that the extra transport has its source in these axially trapped particles.

The variation of $\Delta\omega$ with r/R and ϕ_{cw} is shown in Fig. 8. Figure 8(a) shows that $\Delta\omega$ decreases with radius and increases with $|\phi_{cw}|$. In Fig. 8(b), we show a scaled version of these data demonstrating an empirical relation $\Delta\omega = C|\phi_{cw}|^{0.77}(R/r)^{2.35}$ with $C = 2.70 \times 10^{-3}\text{Mrad}/(\text{s} \cdot \text{V}^{0.77})$.

Finally, we note that the amount of extra transport given by D_{net} also varies with radius and center wire bias. To facilitate a comparison with the transport expected from resonant

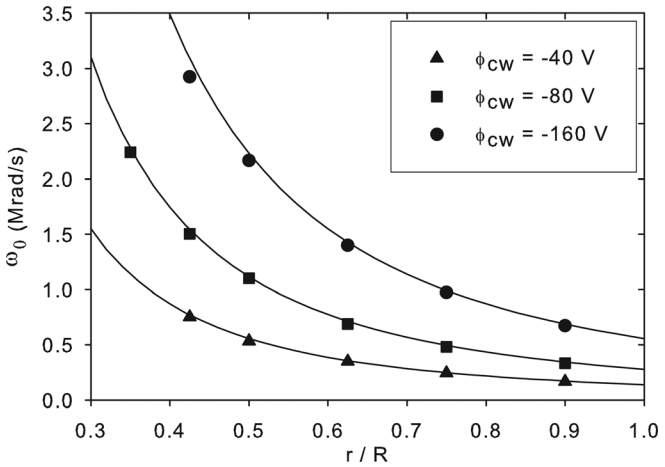

FIG. 7. The filled symbols show the variation of center frequency ω_0 with scaled radius r/R and center wire bias ϕ_{cw}. The simulation data follow closely the calculated variation of the rotation frequency ω_R, shown by the solid lines.

particle theory, we plot in Fig. 9 the ratio $D_{net}/2D_{hel}$ at frequency ω_1 versus r/R for three center wire biases. Figure 9(a) shows the raw data, showing that the ratio increases with radius and decreases with $|\phi_{cw}|$. We have also plotted a dashed line where the ratio is one to show that for most radii, the extra transport is comparable to or larger than the transport expected from resonant particle theory. We also display an empirical scaling of this data in Fig. 9(b) showing that, to good approximation, $D_{net}/2D_{hel} = C(r/R)^{3.86}/|\phi_{cw}|^{0.87}$ with $C = 750\,\mathrm{V}^{0.87}$.

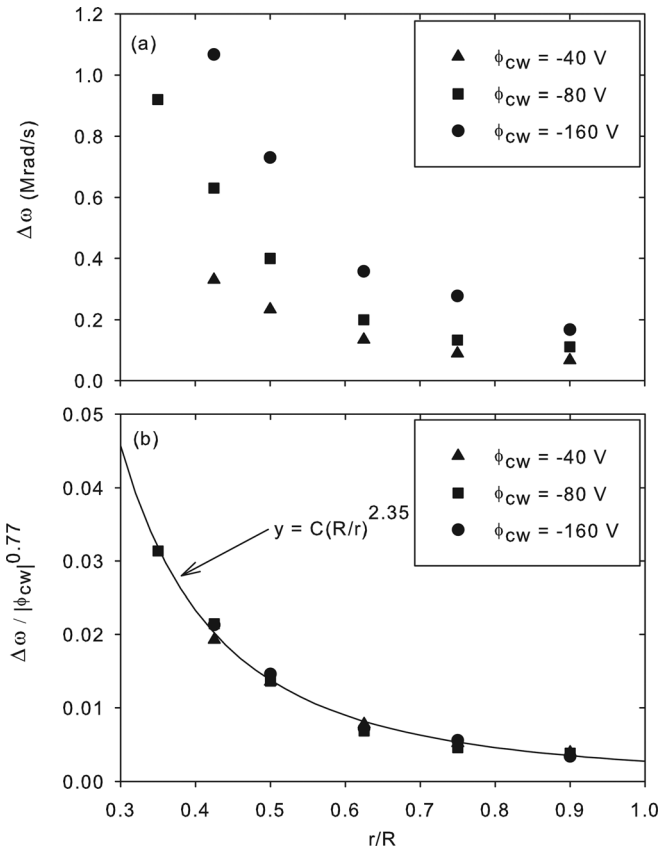

FIG. 8. Variation of $\Delta\omega$ with r/R and ϕ_{cw}. Plot (a) shows the raw data and plot (b) shows an empirical scaling of the data.

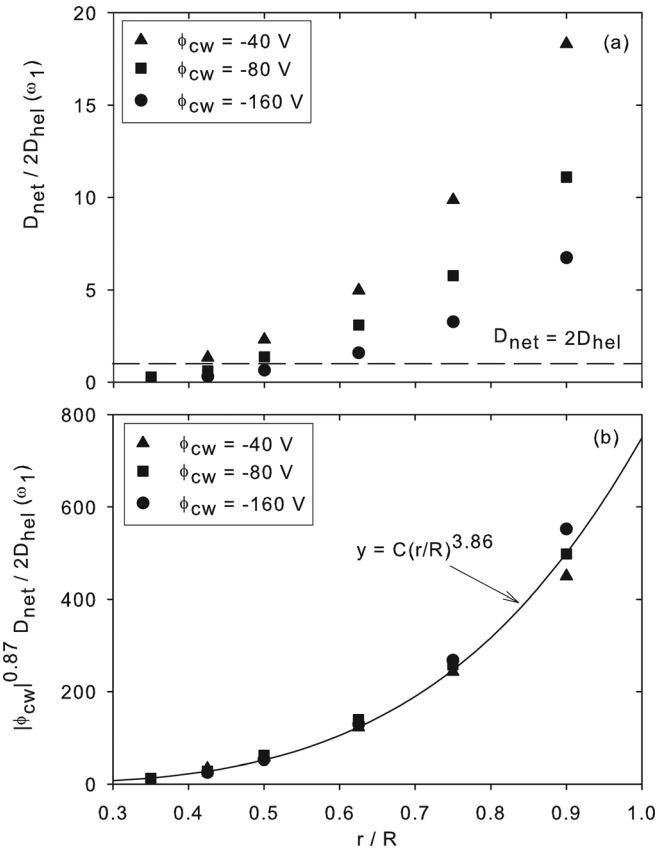

FIG. 9. Variation of $D_{net}/2D_{hel}$ with r/R and ϕ_{cw}. Plot (a) shows the raw data and plot (b) shows an empirical scaling of the data.

V. DISCUSSION

Our results show that, in general, there are two types of asymmetry-induced transport. The first type is described by resonant particle transport theory. In this type of transport, the largest radial excursions occur for particles with velocities near the phase velocities of the helical components of the asymmetry. The second type we will call trapped particle transport. The simulation shows that this type of transport occurs for standing wave asymmetries near radii where $\omega = \omega_R$. From our previous studies,[11] we know that the largest radial excursions occur for particles with velocities low enough to be axially trapped by the asymmetry potential. As Fig. 9 shows, for our experimental conditions, this type of transport is comparable to or larger than the contribution from resonant particle transport and typically dominates at large radii. It is thus not surprising that our previous comparisons of experiment and resonant particle theory have shown serious discrepancies.

As noted in Sec. IV B, the trapped particle transport vanishes for higher collision frequencies. Although we do not fully understand this result, the following explanation seems plausible. While for collisionless conditions, the axially trapped particles have larger radial excursions than the resonant particles, their radial oscillation frequency is significantly lower than ω_T. For higher collision frequencies, it is then possible for the resonant particles to have larger radial excursions than the axially trapped particles, since these latter particles only execute a fraction of their radial orbit in the

time ν^{-1}. Thus, the transport due to resonant particles dominates at higher collision frequencies.

The empirical scalings for $\Delta\omega$ and $D_{net}/2D_{hel}$ shown in Figs. 8(b) and 9(b) are not simple enough to draw firm conclusions, but given that $\omega_R \propto |\phi_{cw}|/r^2$, they suggest a dependence on ω_R or it derivatives with respect to r.

Another interesting feature of this trapped particle transport is the breakdown of the Einstein relation (Eq. (20)) as shown in Fig. 5(b). We see that v_D obtained from the simulation is much larger (10-50 times larger) than predicted by Eq. (20). Note, however, that the Einstein relation is derived assuming an equilibrium velocity distribution. The existence of axially trapped particles invalidates this assumption, so there is no reason to expect the relation to hold.

Even more interesting is the discrepancy between the simulation and our previous experimental work.[15] As just noted, the simulation gives v_D 10-50 times larger than expected from the Einstein relation, whereas our experiments show v_D about ten times *smaller* than expected. Since both simulation and experiment presumably have similar trapped particle distributions, it is hard to see how this discrepancy can be explained by invoking the breakdown of the equilibrium velocity distribution. Instead, we suspect this discrepancy is due to the breakdown of the local approximation. The axially trapped particles in the simulation have radial excursions large enough to be comparable to other radial scale lengths, so the equations used to calculate D and v_D may become invalid.

VI. CONCLUSION

We have found radial particle transport coefficients for asymmetry-induced transport via a single-particle simulation with collisions. The results match resonant particle transport theory for the simple case of a helical asymmetry with periodic boundary conditions. For the more realistic case of a standing wave asymmetry, we have identified a second type of transport that often dominates the resonant particle contribution. This trapped particle transport occurs near radii where $\omega = \omega_R$ and is produced by particles with low enough velocity to be axially trapped by the asymmetry. This second contribution to the transport may explain the discrepancies between experiments and resonant particle theory.

ACKNOWLEDGMENTS

This material is based upon work supported by the Department of Energy under Award No. DE-FG02-06ER54882 and National Science Foundation Grant PHY-1003952.

APPENDIX A: RELATING RANDOM WALK TO COLLISION FREQUENCY

Collisions can be modeled in a single-particle code by a combination of random steps in the velocity and the addition of a drag term in the equation of motion. The random steps in velocity uniformly distributed between $-v_0$ and $+v_0$ are applied with each time step. As is well known, such a random walk produces a velocity distribution that broadens in time. To counteract this and maintain an equilibrium distribution, the drag force $-m\nu v_z$ is added to the equation of motion. It remains to relate the collision frequency ν to the random walk limit v_0.

If the random walk has a uniform weighting w_0, then the normalization condition gives $w_0 = (2v_0)^{-1}$. The average displacement in velocity space $\bar{v}$ due to the random walk is zero, while the mean square displacement after N steps is

$$N\overline{(\Delta v)^2} = N\int_{-v_0}^{v_0} w_0(v-\bar{v})^2 dv = \frac{N}{2v_0}\int_{-v_0}^{v_0} v^2 dv = \frac{Nv_0^2}{3}. \tag{A1}$$

On the other hand, a detailed analysis of the fluctuations modeling collisions in the Langevin equation gives[14]

$$\overline{(\Delta v)^2} = \frac{2kT}{m}\nu\tau, \tag{A2}$$

where τ is a time macroscopically small but large compared to Δt. For our case, we take $\tau = N\Delta t$. Comparing Eqs. (A1) and (A2), we obtain

$$v_0^2 = \frac{6kT}{m}\nu\Delta t. \tag{A3}$$

This gives the random step limits in terms of other chosen parameters.

APPENDIX B: OBTAINING D AND v_D FROM RESONANT PARTICLE THEORY

Here, we include some details on evaluating the theoretical expressions in Sec. III for the asymmetries used in the simulation. Note that, for a helical asymmetry, we have

$$\begin{aligned}\phi_{hel}(r,\theta,z,t) &= \phi_1(r)\cos\left(\frac{n'\pi}{L}z - l'\theta + \omega' t\right)\\ &= \frac{\phi_1(r)}{2}\left\{\exp\left[i\left(\frac{n'\pi}{L}z - l'\theta + \omega' t\right)\right]\right.\\ &\quad\left.+\exp\left[-i\left(\frac{n'\pi}{L}z - l'\theta + \omega' t\right)\right]\right\}.\end{aligned} \tag{B1}$$

Then, Eq. (14) gives

$$\begin{aligned}\phi_{n,l,\omega}(r) = \frac{\phi_1(r)}{2}&\int_{-L}^{L}\frac{dz}{2L}\int_0^{2\pi}\frac{d\theta}{2\pi}\int_0^{\tau}\frac{dt}{\tau}\\ &\times\left[\exp\left[i\left(\frac{\pi z}{L}(n+n') + (l-l')\theta - (\omega-\omega')t\right)\right]\right.\\ &\left.+\exp\left[i\left(\frac{\pi z}{L}(n-n') + (l+l')\theta - (\omega+\omega')t\right)\right]\right].\end{aligned} \tag{B2}$$

The integrand in Eq. (B2) is separable and each of the three integrals produces a delta-function in the corresponding mode number. For example,

$$\begin{aligned}\int_{-L}^{L}\frac{dz}{2L}\exp\left[i\frac{\pi z}{L}(n+n')\right] &= 2i\sin[\pi(n+n')]\\ &= 0 \text{ for n} + n' \neq 0\\ &= \int_{-L}^{L}\frac{dz}{2L}\\ &= 1 \text{ for } n+n'=0\\ &= \delta(n+n').\end{aligned}$$

Thus, Eq. (B2) becomes

$$\begin{aligned}\phi_{n,l,\omega}(r) = \frac{\phi_1(r)}{2}&[\delta(n+n')\delta(l-l')\delta(\omega-\omega')\\ &+\delta(n-n')\delta(l+l')\delta(\omega+\omega')].\end{aligned} \tag{B3}$$

When this result is used in Eqs. (17), (18), and (20), the triple infinite sum in Eq. (15) produces two terms, one with $n, l, \omega = -n', l', \omega'$ and one with $n, l, \omega = n', -l', -\omega'$. The expressions for $D_{nl\omega}$ and $V_{nl\omega}$, however, are unchanged when n, l, and ω all change sign, so the two terms are the same. Thus, for a helical asymmetry of the form of Eq. (2), the procedure for calculating the diffusion coefficients D and v_D from resonant particle theory can be summarized as follows: use Eq. (17) or Eq. (18) with $n, l, \omega = -n', l', \omega'$ and $\phi_{n,l,\omega}(r) = \frac{\phi_1(r)}{2}$, and then double the result to obtain D. Then, use this result in Eq. (20) to obtain v_D.

A similar analysis is used for the case of a standing wave asymmetry of the form of Eq. (3). For this case, we note that

$$\begin{aligned}\phi_{sw}(r,\theta,z,t) &= 2\phi_1(r)\cos\left(\frac{n'\pi}{L}z\right)\cos(-l\theta+\omega t)\\ &= \phi_1(r)\left[\cos\left(\frac{n'\pi}{L}z - l'\theta + \omega' t\right)\right.\\ &\quad\left.+\cos\left(\frac{-n'\pi}{L}z - l'\theta + \omega' t\right)\right].\end{aligned} \tag{B4}$$

Each of the cosine terms is then analyzed as in Eq. (B2) resulting in

$$\begin{aligned}\phi_{n,l,\omega}(r) = \frac{\phi_1(r)}{2}&\left[\delta(n+n')\delta(l-l')\delta(\omega-\omega')\right.\\ &+\delta(n-n')\delta(l+l')\delta(\omega+\omega')\\ &+\delta(n-n')\delta(l-l')\delta(\omega-\omega')\\ &\left.+\delta(n+n')\delta(l+l')\delta(\omega+\omega')\right].\end{aligned} \tag{B5}$$

The analysis then proceeds as before with the additional observation that the expressions for $D_{nl\omega}$ and $V_{nl\omega}$ are also unchanged when n alone changes sign. The procedure for calculating the diffusion coefficients for our standing wave asymmetry can then be summarized as follows: use Eq. (17) or Eq. (18) with $n, l, \omega = -n', l', \omega'$ and $\phi_{n,l,\omega}(r) = \frac{\phi_1(r)}{2}$, and then *quadruple* the result to obtain D.

[1]D. L. Eggleston, T. M. O'Neil, and J. H. Malmberg, Phys. Rev. Lett. **53**, 982 (1984).
[2]J. Notte and J. Fajans, Phys. Plasmas **1**, 1123 (1994).
[3]X.-P. Huang, F. Anderegg, E. M. Hollman, C. F. Driscoll, and T. M. O'Neil, Phys. Rev. Lett. **78**, 875 (1997).
[4]J. M. Kriesel and C. F. Driscoll, Phys. Rev. Lett. **85**, 2510 (2000).
[5]D. L. Eggleston and B. Carrillo, Phys. Plasmas **9**, 786 (2002).
[6]E. Gilson and J. Fajans, Phys. Rev. Lett. **90**, 015001 (2003).
[7]D. L. Eggleston and B. Carrillo, Phys. Plasmas **10**, 1308 (2003).
[8]J. R. Danielson and C. M. Surko, Phys. Plasmas **13**, 055706 (2006).
[9]Y. Soga, Y. Kiwamoto, and N. Hashizume, Phys. Plasmas **13**, 052105 (2006).
[10]D. L. Eggleston and T. M. O'Neil, Phys. Plasmas **6**, 2699 (1999).
[11]D. L. Eggleston, Phys. Plasmas **14**, 012302 (2007).
[12]R. Hornbeck, *Numerical Methods* (Quantum, New York, 1975), pp. 194–196.
[13]D. H. E. Dubin, Phys. Plasmas **15**, 072112 (2008).
[14]F. Reif, *Fundamentals of Statistical and Thermal Physics* (McGraw-Hill, New York, 1965), pp. 560–575.
[15]D. L. Eggleston, Phys. Plasmas **17**, 042304 (2010).